Tailoring the Surface Chemistry of Gold Nanorods through Au–C/Ag–C Covalent Bonds Using Aryl Diazonium Salts

ARTICLE *in* THE JOURNAL OF PHYSICAL CHEMISTRY C · JULY 2014

Impact Factor: 4.77 · DOI: 10.1021/jp504040d

THE JOURNAL OF PHYSICAL CHEMISTRY C

Article

pubs.acs.org/JPCC

Tailoring the Surface Chemistry of Gold Nanorods through Au−C/Ag−C Covalent Bonds Using Aryl Diazonium Salts

Randa Ahmad,[†] Leïla Boubekeur-Lecaque,*[,†] Mai Nguyen,[†] Stéphanie Lau-Truong,[†] Aazdine Lamouri,[†] Philippe Decorse,[†] Anouk Galtayries,[‡] Jean Pinson,[†] Nordin Felidj,[†] and Claire Mangeney*[,†]

[†]ITODYS, UMR 7086 CNRS, Univ. Paris Diderot, Sorbonne Paris Cité, 15 rue J-A de Baïf, 75205 Paris Cedex 13, France

[‡]Laboratoire de Physico-Chimie des Surfaces, CNRS-ENSCP (UMR 7045), Chimie ParisTech, 11 rue Pierre et Marie Curie, F-75005 Paris, France

Supporting Information

ABSTRACT: Tailoring the surface chemistry of gold nanorods is a key factor for successful applications in biology, catalysis, and sensing. Here, we report on the use of the diazonium salt chemistry for the functionalization of gold nanorods enabling the formation of strongly attached organic layers around the gold cores. The precise nature of the interface between the gold surface and the diazonium-derived aryl layers was probed by XPS, ToF-SIMS, SERS, and DFT. It was shown that the CTAB surfactant was partially exchanged by the diazonium salt which dediazonizes spontaneously to form Au−C covalent bonds with the surface. Interestingly, the silver used during the synthesis of gold nanorods and still present at their surface appears to be also involved in the grafting mechanism with Ag−C covalent bonds detected by ToF-SIMS. From this result, it is clear that the interfacial properties and reactivity of gold nanorods synthesized by the silver(I)-assisted seed mediated growth approach are strongly influenced by the presence of silver.

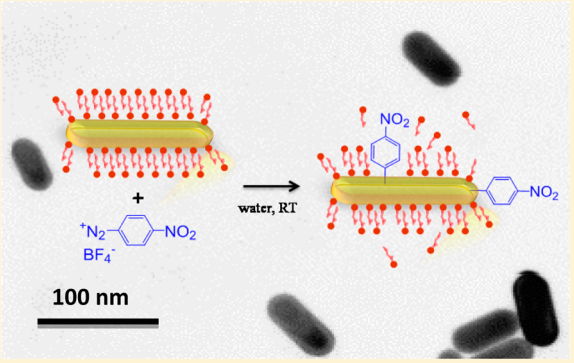

INTRODUCTION

Gold nanoparticles have stimulated a wide range of interest these past years due to their potential applications in many fields such as biology,[1−3] catalysis,[4,5] electronics,[6,7] and optics.[8,9] Anisotropic gold nanorods (GNRs) have specifically received a great deal of attention due to their large absorption cross section in the visible and near-infrared frequencies which opens new opportunities for localized hyperthermia in cancer therapeutics.[10,11] Their use generally requires their functionalization in order to protect colloidal particles from aggregation and to manipulate the optical,[12−14] electronic,[10,15,16] and catalytic[17] properties of the gold core, as well as to control interfacial properties. Although the self-assembly of alkythiolate monolayers is the most widely applied modification method for gold surfaces, the noncovalent nature of the Au−S interaction may impart some instability to the interface.[18−20] For example, these monolayers are thermally unstable and are prone to displacement by other thiols and ambient UV photooxidation.[21]

As an alternative to alkanethiol self-assembled monolayers (SAMs), diazonium salts have been recently proposed for the modification of metallic surfaces, from planar ones to nanoparticles.[22−25] Strongly attached disordered mono- or multilayers are obtained by this method, the interaction between diazonium-derived aryl films and the gold surface being very stable.[26,27] The mechanism of the electroless grafting reaction on gold surfaces has been debated. Aryl radicals, aryl cations, and diazonium cations grafting on the gold surface have been proposed.[28] The stability of the grafted organic layer relies on the formation of a carbon−gold covalent bond and drives the examination of diazonium-derived layers as an alternative to SAMs for applications where extremely stable surface chemistry is required. If the formation of a gold−carbon covalent bond was postulated once, real experimental proofs of its existence were obtained only very recently. For this, McDermott et al. used a combination of DFT modeling and SERS experiments on citrate-capped spherical (isotropic) gold nanoparticles functionalized by nitrophenyl groups derived from diazonium salts.[25] From their results, they could assign the 412 cm^{-1} band to the Au−C stretching mode, confirming the wide potentialities of this functionalization strategy for obtaining strong adsorbate−substrate coupling. Concerning gold nanorods, their functionalization using diazonium salt chemistry has never been reported so far. One could expect that it should be significantly more challenging than the functionalization of spherical particles, due to the unique surfactant capping of as-synthesized nanorods.[29] Indeed, while spherical particles may be directly coated during their synthesis or are coated with weakly bound anions, gold nanorods are usually synthesized in the presence of a cationic surfactant, cetyltrimethylammonium

Received: April 25, 2014
Revised: July 10, 2014
Published: July 10, 2014

   dx.doi.org/10.1021/jp504040d | J. Phys. Chem. C 2014, 118, 19098−19105

bromide (CTAB), which binds more strongly to the nanorod surface. Furthermore, the presence of silver at their surface, originating from their synthesis by the Ag(I)-assisted seed-mediated growth approach, introduces additional complexity in the surface chemistry of these nanoparticles which should be taken into account.[30−33]

In this work, we address this issue by exploring for the first time the potentialities of the diazonium salt chemistry to functionalize colloidal gold nanorods, as illustrated in Scheme 1. As a proof of concept, we chose the 4-nitrobenzenediazonium salt (dNB), a good vibrational probe displaying a strong nitro stretching band. The key challenges are the formation of gold−carbon covalent bonds at the nanorod surface by replacement of the adsorbed CTAB molecules and the preservation of the colloidal stability of the aqueous dispersion following functionalization. Detailed X-ray photoelectron spectroscopy (XPS), time-of-flight secondary ion mass spectrometry (ToF-SIMS), and surface-enhanced Raman spectroscopy (SERS) studies provided important information related to the exact nature of the interface between the GNRs and the organic coating.

Scheme 1. Schematic Illustration of Surface Modification of GNRs Using the Diazonium Salt Chemistry

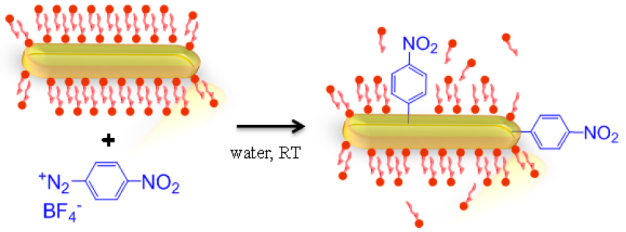

RESULTS AND DISCUSSION

Gold NRs were prepared through the well-known seed-mediated growth procedure, based on the reduction of $HAuCl_4$ with a weak reducing agent (ascorbic acid) on premade CTAB-stabilized Au nanoparticle seeds, in the presence of CTAB and $AgNO_3$. The produced nanorods with an aspect ratio of ca. 2.6 showed an average length L of 50 ± 3 nm and a small axis d of 19 ± 3 nm. In order to functionalize the GNRs by dNB, the method we used consisted of simply adding the diazonium salt (at various concentrations, from 10^{-6} to 10^{-4} M) to the GNRs aqueous dispersions ([GNRs] = 0.7×10^{-9} M) and letting it react during 24 h at room temperature. The functionalized GNRs were then purified through three cycles of centrifugation/redispersion in water. The TEM images, displayed in Figure 1, show that the reaction of the GNRs with dNB does not disturb their colloidal stability with perfectly dispersed particles obtained after functionalization.

The UV−visible spectra of GNRs confirm that their colloidal stability is preserved, without any spectral broadening of the plasmon bands, even after the addition of dNB (see Figure 2). The GNRs suspensions modified with dNB remain stable over time with no evidence of aggregation after at least 1 month. Two extinction bands are observed due to the anisotropy of the particles: a weak maximum emerges around 520 nm, due to the excitation of a localized surface plasmon (LSP) mode along the short axis (transverse mode), and a strong and well-defined LSP mode along the main axis (longitudinal mode) is observed at ∼720 nm. This latter mode is very sensitive to the local environment. As a result, it shifts upon addition of dNB, from 690 to 700 nm, indicating the adsorption of organic layers on GNRs.

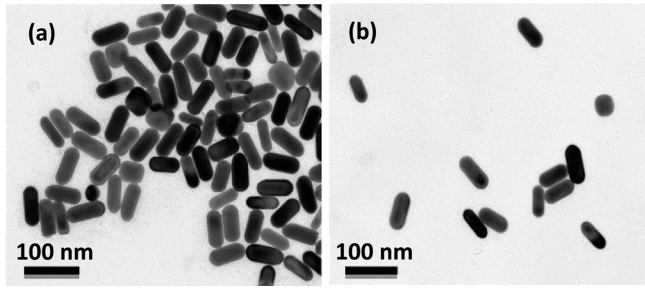

Figure 1. TEM images of GNRs (a) before and (b) after functionalization by dNB.

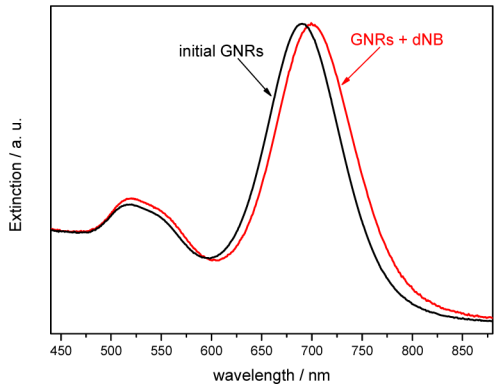

Figure 2. Normalized extinction spectra of colloidal solutions of initial CTAB-coated GNRs (black curve) and functionalized GNRs-NB, after addition of 10^{-4} M dNB (red curve).

In order to study more precisely the chemical modifications induced by the diazonium salts at the surface of GNRs, XPS analysis were performed on bare and functionalized samples. Important changes were detected both (i) on the survey scans and (ii) on the high resolution spectra of N 1s, reflecting a modification of the general chemical composition of the GNRs surface. The survey scan of the initial GNRs, shown in Figure 3a, displays the characteristic peaks of both CTAB (C 1s at 285 eV, N 1s at 402.3 eV, and Br 3d at 67.5 eV), silver (Ag 3d at 367.8 eV), and gold (Au 4f at 84.3 eV). The presence of silver at the surface of GNRs was previously reported by Orendorff and Murphy[34] who suggested that silver metal is mostly distributed on the surface of the particles, in accordance with the underpotential deposition model proposed by Liu and Guyot-Sionnest for gold nanorod growth.[35] After functionalization, the signals assigned to the CTAB layer (Br^- and N^+) decrease progressively as the concentration of dNB increases in the incubation medium. Simultaneously, a strong increase of the gold signal is observed indicating a partial release of the CTAB coating surrounding the GNRs. A close inspection of the N 1s high-resolution spectra indicates that this partial release is accompanied by the appearance of two new components, one of which corresponds to nitro groups (at 406 eV). The other component (at 400 eV) could correspond to diazenyl groups introduced by electrophilic attack of the diazonium cation on aromatic rings (azo coupling reaction).[36,37] This last peak could also be interpreted as the presence of amines as exposure to X-ray irradiation during the XPS analysis could induce a partial reduction of nitro groups into amino groups. It is worth noting

dx.doi.org/10.1021/jp504040d | J. Phys. Chem. C 2014, 118, 19098−19105

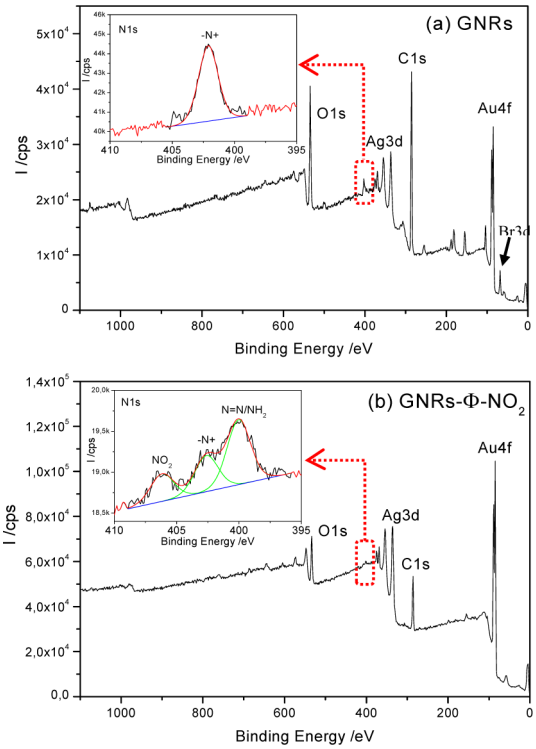

Figure 3. XPS survey spectra of (a) CTAB-coated GNRs and (b) GNRs obtained after reaction with the diazonium salt $^{+}N_2-C_6H_4-NO_2$ (10^{-4} M). The insets show the corresponding high-resolution N 1s spectra.

that no peak that would be attributed to nitrogen atoms from the diazonium group can be observed, evidencing the complete transformation of the diazonium cations. Table 1 summarizes the surface chemical composition of the different samples with varying concentrations of diazonium salt (10^{-6} and 10^{-4} M). The silver content remains constant after functionalization, indicating that it is not removed during the departure of the CTAB surfactant.

Table 1. Surface Chemical Composition (atom %) of Initial GNRs (Coated with CTAB) and GNRs−Ph−NO_2 after Reaction with Various Concentrations of dNB (10^{-6} and 10^{-4} M)

					N		
samples	Au	Ag	Br	C	N^+	NO_2	N=N
GNRs−CTAB	6.5	1	4	84	4.5	−	−
GNRs−Ph−NO_2 10^{-6} M	14	2	2	78	2.5	0.5	1
GNRs−Ph−NO_2 10^{-4} M	19	2	0.5	69	2.5	2	5

Two main conclusions can be drawn from these results. First, the chemical evolution observed at the GNRs surface suggests that the CTAB bilayer surrounding the particles has been disrupted by the introduction of the diazonium salt, in favor of a partial exchange between CTAB and nitrophenyl grafts.

The second important feature is the high intensity of the N=N component in the N 1s signal (~50%), indicating the presence of a large quantity of azo coupling during the grafting reaction. This observation contrasts significantly with the mechanism proposed by McDermott et al. on citrate-capped spherical gold nanoparticles favoring a growth of the nitrophenyl multilayer through aryl−aryl C−C coupling.[25] In the present case, the azo coupling appears to be also involved in the growth of the nitrophenyl layer at the surface of the GNRs through −Ph−N=N−Ph−NO_2 linkages,[38,39] in line with G. Deniau et al.[28]

Nevertheless, the question of the exact nature of the interface between the gold surface and the aryl layer (i.e., Au−C versus Au−N covalent bonds) could not be answered using XPS due to the tiny difference in electronegativity between carbon and gold atoms (χ_C = 2.55 and χ_{Au} = 2.54 using the Pauling scale). Furthermore, due to the presence of silver on the GNR surface, a grafting mechanism involving interfacial Ag−C bonds could also be involved.

In order to get a more precise description of the chemical nature of the Au NP/aryl layer interface, ToF SIMS experiments were performed on the samples. The most significant fragments are reported in Table 2. In all samples, the surfactant is clearly detected with intense peaks due to CTA^+, Br^-, and $AgBr_2^-$ (as a counteranion). After addition of dNB, new peaks appear due to the aryl fragments (NO_2^-, $C_6H_5^+$, $C_6H_4-NO_2^-$). Interestingly, a strong-intensity component corresponding to $Au-Br^-$ fragments is observed for the initial CTAB-coated GNRs while it decreases sharply after dNB treatment. It is replaced by two new components, $Au-C_6H_4-NO_2^+$ and $Ag-C_6H_4-NO_2^+$. The appearance of $Au-C_6H_4-NO_2^+$ signal confirms the partial exchange of CTAB by dNB and the covalent grafting of the aryl groups to the gold surface through Au−C covalent bonds.

Table 2. TOF-SIMS Spectra of Initial CTAB-Coated GNRs and Functionalized GNRs−Ph−NO_2 (Positive and Negative Fragments)

m/z expt	assignment	intensity on CTAB−GNRs	intensity on GNRs−Ph−NO_2
284.346	CTA^+	1896015	1863582
275.854	$Au^{79}Br^-$	163932	13852
277.820	$Au^{81}Br^-$	153259	9390
45.964	NO_2^-	22392	1523572
77.065	$C_6H_5^+$	29098	203565
121.973	$C_6H_4NO_2^-$	2282	118528
229.016	$^{107}Ag-C_6H_4-NO_2^+$	1317	11831
230.991	$^{109}Ag-C_6H_4-NO_2^+$		11131
319.314	$Au-C_6H_4NO_2^+$	489	10468
469.140	$[Au-C_6H_3(NO_2)$-N=N−$C_6H_4(NO_2)$ + H]$^+$	488	10215
332.051	$[^{107}Ag-C_6H_3(NO_2)-N=N-C_6H_4(NO_2)$ + H]$^+$	442	19544
334.051	$[^{109}Ag-C_6H_3(NO_2)-N=N-C_6H_4(NO_2)$ + H]$^+$	885	15338

Surprisingly, this last signal is accompanied by the signature of $Ag-C_6H_4-NO_2^+$ fragments which indicates that the Ag layer present at the surface of the GNRs is also involved in the grafting mechanism, through Ag−C covalent bonds. This result emphasizes the necessity to take into account the presence of this Ag layer at the GNRs surface in order to fully understand their interfacial properties and reactivity. To our knowledge, it is the first direct evidence of a covalent bond between silver and diazonium-derived aryl layers. Grafted oligomers of nitrophenyl with azo linkages are also detected after functionalization, in agreement with XPS analysis.

dx.doi.org/10.1021/jp504040d | J. Phys. Chem. C 2014, 118, 19098−19105

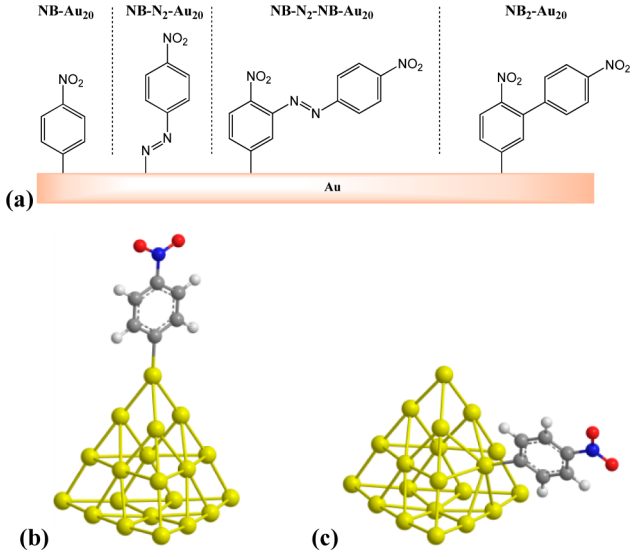

Figure 4. (a) NB adducts envisaged for DFT modeling; NB coordinated to (b) the vertex of the cluster NB−Au_{20}-v; (c) the face of the cluster NB−Au_{20}-f.

The GNRs samples were further characterized by surface-enhanced Raman scattering (SERS) experiments, and the results were compared with the Raman spectra calculated from DFT modeling on different possible grafting adducts. Figure 5 shows the experimental SERS signal for nitrophenyl-modified GNRs and the calculated Raman spectra for various nitrophenyl adducts on gold surface. The SERS spectrum recorded in solution at 785 nm displays mainly five bands in the range 150−2000 cm^{-1} with peak positions at 178, 851, 1109, 1340, and 1589 cm^{-1}. The strong band at 178 cm^{-1} is commonly assigned to the Au−Br bond stretching, originating from the adsorption of CTAB on gold surface.[40] The presence of this band, even after the functionalization of GNRs by the nitrophenyl layers (see Figure S1 in the Supporting Information), indicates that the CTAB molecules are only partially removed, in accordance with XPS results.

The grafting of nitrophenyl groups on the GNRs surface was modeled by a hybrid system based on the pyramidal gold cluster Au_{20}. The spontaneous dediazonation of dNB on gold surface leads to the nitrophenyl−gold adduct through Au−C bond. The most favorable interaction between gold and the nitrophenyl radical, whose singly occupied molecular orbital (SOMO) lies in the molecular aromatic plane, was envisaged in the perpendicular conformation as a σ-type coordination (see Figure 4).

This adsorbed species, standing up on the surface, was modeled by NB−Au_{20} for DFT calculations in two binding configurations where the Au−C bond involves the vertex or one of the four faces of the pyramidal Au_{20} cluster (see Figure 4b,c). These two binding configurations, denoted NB−Au_{20}-f and NB−Au_{20}-v, mimic the coordination of aryl group respectively onto (111) fcc gold face and to an adatom site. The possible formation of NB multilayer was modeled by a biphenyl derivative NB_2 coordinated to the cluster. NB−Au_{20}-v and NB−Au_{20}-f have the same Raman band positions but the corresponding intensities differ widely (see Supporting Information). In particular, the vibration located at 851 cm^{-1} in the SERS spectrum is significantly weaker for the aryl bonded to the face than to the vertex of Au_{20}. Besides nitro scissoring mode, the vibration at 851 cm^{-1} involves also the

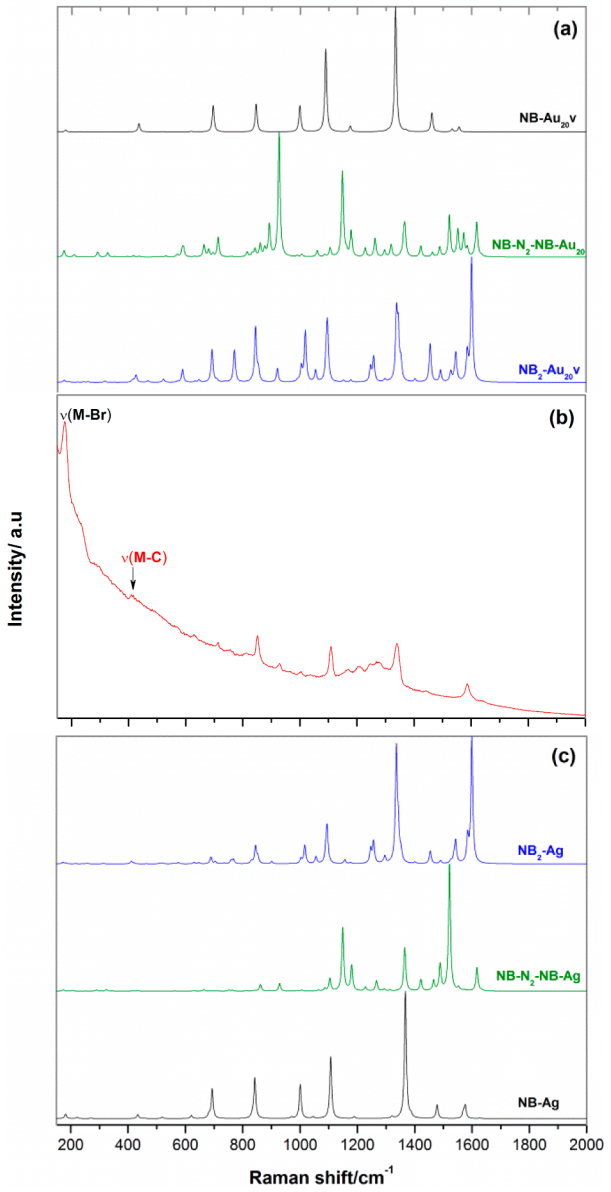

Figure 5. (b) Experimental SERS spectrum of nitrophenyl on gold nanorods in solution at 785 nm (red) and the calculated Raman spectra of NO_2−aryl on (a) gold cluster Au_{20} for NB−Au_{20}-v (black), NB_2−Au_{20}-v (blue), and NB−N_2−NB−Au_{20} (green); and (c) on Ag for NB−Ag (black), NB_2−Ag (blue), NB−N_2−NB−Ag (green).

motion of the carbon atom along the C−Au bond and in-plane C−H bending in α-position. This mode is therefore expected to be influenced by the interaction with gold which experiences different chemical environments in the face and the vertex of Au_{20}.

Among the two possible binding modes on the gold cluster, NB bonded to the vertex of the pyramid (NB−Au_{20}-v) proved to be more stable by 8.2 kcal·mol^{-1} than the configuration bonded to the face of the pyramid (NB−Au_{20}-f). For the sake of clarity and since the band positions are similar for both configurations, the DFT -simulated spectra will only be discussed for the vertex model.

The confrontation of the SERS spectrum recorded on GNRs with the DFT-simulated Raman spectra on NB−Au_{20} and NB_2−Au_{20} models (see Table 3) shows that the biphenyl adduct NB_2 is the best model in this case. Indeed, the observed

dx.doi.org/10.1021/jp504040d | J. Phys. Chem. C 2014, 118, 19098−19105

Table 3. Raman Bands Assignment of SERS Spectrum for Nitrobenzene Diazonium on GNRs

exptl/cm^{-1}	calcd/cm^{-1}					
SERS on GNRs	NB−Au_{20}	NB_2−Au_{20}	NB−N_2−NB−Au_{20}	NB−Ag	NB_2−Ag	assignment[a]
1589	1558	1602		1581	1603	ν(C═C) ring
		1549			1546	ν(C═C) ring, $\nu_{asym}(NO_2)$
	1463	1460		1483	1446	ν(C═C) ring, δ_{ip} (C−H)
1341	1338	1342		1370	1340	$\nu_{sym}(NO_2)$
		1258			1258	δ_{ip} (C−H)
			1152			δ_{ip} (C−H)
1109	1092	1097		1110	1098	ν(C−N), δ_{ip} (C−H)
926	–		928			C−N═N scissoring, δ_{oop} (C−H), ν(Au−C)
851	848	845		846	846	ONO scissoring, δ_{ip} (C−H), ν(Au−C)
	696	692		695		δ_{oop} (C−H), δ_{oop} (NO_2)
413	435	424		435	414	ν(C−M)
178	–	–	–	–	–	ν(Au−Br)

[a] ν, stretching; δ_{ip} (δ_{oop}), in-plane (out of plane) bending; M = Ag or Au.

band at 1589 cm^{-1} is only reproduced by the NB_2−Au_{20}-v model (band predicted at 1602 cm^{-1}). Although a number of weaker additional bands are predicted for NB_2−Au_{20}-v but not apparent in the SERS spectrum, the four main bands observed experimentally in the range 600−2000 cm^{-1} are faithfully reproduced in terms of Raman shift (within ca. 5−10 cm^{-1}).

In addition to the binding mode of gold surface via the carbon atom resulting from the radical mechanism, the grafting of diazonium salt on gold was also envisaged for the cationic mechanism leading to the formation of N−Au bond and/or N═N multilayer (NB-N_2−Au_{20} and NB-N_2−NB-Au_{20} model systems, see Figure 4a). For the NB-N_2−Au_{20} model system, a strong band at 1763 cm^{-1} is predicted for the N═N bond stretch (see Supporting Information). Given that this strong Raman band was not revealed in the experimental SERS spectra and there was no contribution of N−Au to the XPS N 1s signal, the grafting of diazonium salt through N−Au bond on GNRs was then definitely ruled out. Conversely, as evidenced by McDermott on citrate-capped gold nanoparticles, a band of low intensity at 413 cm^{-1} is apparent in the SERS spectrum of functionalized GNRs. This mode assigned to Au−C stretch points to a spontaneous dediazonation of the nitrobenzene diazonium leading to aryl coordination on gold surface through C−Au bond.

Based on the high-resolution XPS analysis of N 1s signal (vide supra), the possible involvement of azo coupling in the multilayer growth was taken into account by modeling NB−N═N−NB−Au_{20}. The simulated Raman spectrum for such species exhibits a complex vibrational signature where two strong bands at 1150 and 928 cm^{-1} stand out. Although being weak in the SERS spectrum, a band at 926 cm^{-1} appears upon 4-nitrobenzene diazonium grafting which substantiates the presence of azo coupling adducts. The low intensity of this band could seem in contradiction with the large proportion of azo component in the N 1s XPS signal. However, considering that SERS is a near-field technique where the Raman intensity decays exponentially with the distance, it becomes clear that the obtained SERS signal reflects only the first layers of the thin organic film grown onto gold surface.

Given that silver is unambiguously evidenced by XPS and TOF-SIMS analysis on NB modified GNRs, the same NB adducts coordinated to silver were examined by DFT and the corresponding simulated spectra are represented in Figure 5c. One may notice the strong similarities between the simulated spectra for NB−Au_{20}-v and NB−Ag models. This is likely due to the fact that the vertex of Au_{20} cluster represents Au adatom behaving roughly as a single Ag atom. As interpreted previously for Au_{20} adducts, it appears that the simulated Raman spectra for the biphenyl NB_2−Ag model reproduce all the spectral features of the SERS spectrum. The metal−carbon bond stretching mode located at 413 cm^{-1} on the SERS spectra is predicted at 435 and 414 cm^{-1} for NB−Ag and NB_2−Ag, respectively. Regarding the azo adduct on silver NB−N═N−NB−Ag, there is no conclusive evidence from the SERS analysis sustaining this mechanism.

To summarize the combined DFT and SERS analysis, the reaction of GNRs with nitrophenyldiazonium salt leads to a multilayer thin film of nitrophenyl where the first aryl group is bonded via the C atom to both Ag and Au present on the surface. Multilayer growth via azo coupling may be involved on gold but direct attachment of diazonium group through Au−N bond[28] is definitely ruled out in the present example.

CONCLUSION

In this study, we have explored the potentialities of the aryl diazonium salt chemistry for functionalizing gold nanorods. The approach is very simple as it consists of simply adding the diazonium salt, here 4-nitrophenyldiazonium, to the GNRs dispersion in water and letting it react at room temperature. The colloidal stability is preserved during functionalization, although the spectroscopic analysis indicated the partial removal of the CTAB surfactant initially covering the GNRs. The nitrophenyl layers were grafted at the surface of GNRs through covalent Au−C bonds as observed from TOF-SIMS and SERS analysis, combined to DFT calculations. Interestingly, the silver layer present at the GNRs surface, originating from their synthesis by the commonly used silver(I)-assisted seed-mediated growth approach, was shown to be also involved in the surface reactivity of the particles. Indeed, it remains on the GNR surface even after CTAB removal and forms covalent Ag−C bonds with the diazonium-derived aryl layers, as evidenced for the first time by TOF-SIMs. These results highlight the efficiency of the diazonium salt chemistry to spontaneously functionalize gold nanorods through covalent bonds and therefore open new opportunities for the preparation of aryl-layers-coated plasmonic nanoparticles. In order to achieve biocompatible GNRs, the full replacement of CTAB layer is required. Our group is currently exploring other diazonium salts allowing the complete replacement of CTAB

dx.doi.org/10.1021/jp504040d | J. Phys. Chem. C 2014, 118, 19098−19105

while maintaining the colloidal stability. The results will be reported in due course.

EXPERIMENTAL SECTION

Materials. Chloroauric acid ($HAuCl_4$) was purchased from Alfa Aesar. Hexadecyltrimethylammonium bromide CTAB (98%), sodium borohydride (99%), silver nitrate, and L-ascorbic acid were purchased from Sigma-Aldrich. Deionized water (18 MΩ) was used in all the experiments. For preparation of GNRs, seed and growth solutions were made as described below.

Synthesis of Gold Nanorods. The GNRs were prepared via the seed growth method, as described by El Sayed et al.[29] Briefly, the seed solution was prepared by mixing a CTAB solution (5 mL, 0.20 M) with aqueous $HAuCl_4$ (5 mL, 0.5 mM). To this mixture, 0.6 mL of ice-cold $NaBH_4$ solution (0.01 M) was added dropwise and the mixture was vigorously stirred for 2 min which resulted in a brownish yellow solution of small seed gold particles (2−5 nm). The seed solution was kept at 25 °C. In order to grow GNRs, the procedure was as follows. In a separate flask, a 1 mL of $AgNO_3$ (4 mM) was added to a CTAB solution (50 mL, 0.2 M) at 35 °C. Then 50 mL of 1 mM of $HAuCl_4$ was added to the previous solution and mixed. To this solution, 0.7 mL of 78 mM ascorbic acid was added, changing the color of the growth solution from yellow brown to colorless. The final step was the addition of 120 μL of the seed solution to the growth solution at 27−35 °C. The color of the solution gradually changed within 10−20 min. GNRs were purified by two centrifugation steps (20 min, 5000 rpm) for elimination of excess of surfactant and unreacted products and were redispersed in deionized water.

Functionalization of Gold Nanorods. The 50 nm GNRs in aqueous solution (OD = 0.3, [GNRs] = 0.7×10^{-9} M) were modified by adding 10^{-4} M of 4-nitrobenzendiazonium tetrafluoroborate. The mixture was left to incubate for 24 h at room temperature and then the nanorods were separated from solution via centrifugation at 4700 rpm for 10 min. Next, the GNRs were redispersed in 1 mL of deionized water. The suspended modified particles were stable and stored at 7 °C until use.

Instrumentation. XPS spectra were recorded using a Thermo VG Scientific ESCALAB 250 system fitted with a microfocused, monochromatic Al Kα X-ray source ($h\nu$ = 1486.6 eV; spot size = 650 μm; power =15 kV × 200 W). The pass energy was set at 150 and 40 eV for the survey and the narrow regions, respectively. An electron flood gun was used, under a 2×10^{-8} mbar partial pressure of argon, for static charge compensation. These conditions resulted in negative but uniform static charge. Spectral calibration was determined by setting the main C 1s component at 285 eV. The surface composition was determined using the integrated peak areas and the corresponding Scofield sensitivity factors corrected for the analyzer transmission function. The LSPR resonance of these systems was probed by using far-field visible−NIR extinction microspectroscopy in the range of 450−900 nm. Transmission electron microscopy (TEM) characterizations were performed using a Jeol 100-CX II microscope, operating at 100 kV. The concentrated GNRs were first dispersed in water and one drop of this dispersion was deposited on a carbon grid.

Raman spectra were recorded in solution on a confocal Raman microspectrometer (Jobin-Yvon LABRAM HR 800) fed with 785 nm laser line. The objective used in this backscattering setup is a 50× (NA = 0.75). The Raman spectra are recorded within the spectral range of 100−2000 cm^{-1}, with an acquisition time varying from 30 to 90 s.

Time-of-flight secondary-ion mass spectrometry (TOF-SIMS) data were acquired using a TOF-SIMS V spectrometer (ION-TOF GmbH). The analysis chamber was maintained at less than 5×10^{-7} Pa under operating conditions. The total primary ion flux was below 10^{12} ions cm^2 to ensure static conditions. A pulsed 25 keV Bi^+ primary ion source (Liquid Metal Ion Gun, LMIG) at a current of about 1 pA (high current bunched mode), raster over a scan area of 500 × 500 μm, was used as the analysis beam.

Computational Details. All calculations were carried out using the Gaussian 09 suite of programs[41] using the B3LYP exchange and correlation functional[42,43] along with the 6-311++G(d,p) basis set for all atoms but gold.[44,45] The LANL2DZ basis set consisting of Effective Core Potential (ECP) and double-ζ quality functions for valence electrons was employed for Au.[46] The structures were optimized without symmetry constraint (see Supporting Information). The vibrational frequencies and normal modes were calculated within the harmonic approximation, and a scaling factor of 0.976 was chosen on the basis of previously published work.[47]

ASSOCIATED CONTENT

Supporting Information

Computational section and SERS spectra of as-synthesized gold nanorods. This material is available free of charge via the Internet at http://pubs.acs.org.

AUTHOR INFORMATION

Corresponding Authors

*E-mail: claire.mangeney@univ-paris-diderot.fr. Phone: +33-1-57276878. Fax: 33-01-57277263.

*E-mail: leila.boubekeur@univ-paris-diderot.fr. Phone: +33-1-57278772. Fax: 33-01-57277263.

Notes

The authors declare no competing financial interest.

ACKNOWLEDGMENTS

The authors are indebted to L. Mouton from ITODYS for his technical support on TEM-HRTEM facilities.

ABBREVIATIONS

GNRs, gold nanorods; XPS, X-ray photoelectron spectroscopy; TEM, transmission electron microscopy; SERS, surface-enhanced Raman spectroscopy; TOF-SIMS, time-of-flight secondary ion mass spectrometry; DFT, density functional theory

REFERENCES

(1) Mukherjee, P.; Bhattacharya, R.; Wang, P.; Wang, L.; Basu, S.; Nagy, J. A.; Atala, A.; Mukhopadhyay, D.; Soker, S. Antiangiogenic Properties of Gold Nanoparticles. *Clin. Cancer Res.* **2005**, *11*, 3530−3534.

(2) Giljohann, D. A.; Mirkin, C. A. Drivers of Biodiagnostic Development. *Nature* **2009**, *462*, 461−464.

(3) Patra, C. R.; Bhattacharya, R.; Mukhopadhyay, D.; Mukherjee, P. Application of Gold Nanoparticles for Targeted Therapy in Cancer. *J. Biomed. Nanotechnol.* **2008**, *4*, 99−132.

(4) Yuan, Y. Z.; Asakura, K.; Wan, H. L.; Tsai, K. R.; Iwasawa, Y. Supported Gold Catalysts Derived from Gold Complexes and as-

Precipitated Metal Hydroxides, Highly Active for Low-Temperature Co Oxidation. *Chem. Lett.* **1996**, 755−756.
(5) Sakurai, H.; Haruta, M. Synergism in Methanol Synthesis from Carbon Dioxide over Gold Catalysts Supported on Metal Oxides. *Catal. Today* **1996**, *29*, 361−365.
(6) Chandrasekharan, N.; Kamat, P. V. Improving the Photoelectrochemical Performance of Nanostructured TiO(2) Films by Adsorption of Gold Nanoparticles. *J. Phys. Chem. B* **2000**, *104*, 10851−10857.
(7) Nakai, H.; Yoshihara, M.; Fujihara, H. New Electroactive Tetrathiafulvalene-Derivatized Gold Nanoparticles and Their Remarkably Stable Nanoparticle Films on Electrodes. *Langmuir* **1999**, *15*, 8574−8576.
(8) Elghanian, R.; Storhoff, J. J.; Mucic, R. C.; Letsinger, R. L.; Mirkin, C. A. Selective Colorimetric Detection of Polynucleotides Based on the Distance-Dependent Optical Properties of Gold Nanoparticles. *Science* **1997**, *277*, 1078−1081.
(9) Leroux, Y.; Lacroix, J. C.; Fave, C.; Trippe, G.; Felidj, N.; Aubard, J.; Hohenau, A.; Krenn, J. R. Tunable Electrochemical Switch of the Optical Properties of Metallic Nanoparticles. *ACS Nano* **2008**, *2*, 728−732.
(10) Huang, H. C.; Rege, K.; Heys, J. J. Spatiotemporal Temperature Distribution and Cancer Cell Death in Response to Extracellular Hyperthermia Induced by Gold Nanorods. *ACS Nano* **2010**, *4*, 2892−2900.
(11) Dickerson, E. B.; Dreaden, E. C.; Huang, X. H.; El-Sayed, I. H.; Chu, H. H.; Pushpanketh, S.; McDonald, J. F.; El-Sayed, M. A. Gold Nanorod Assisted near-Infrared Plasmonic Photothermal Therapy (Pptt) of Squamous Cell Carcinoma in Mice. *Cancer Lett.* **2008**, *269*, 57−66.
(12) Wang, H. F.; Huff, T. B.; Zweifel, D. A.; He, W.; Low, P. S.; Wei, A.; Cheng, J. X. In Vitro and in Vivo Two-Photon Luminescence Imaging of Single Gold Nanorods. *Proc. Natl. Acad. Sci. U.S.A.* **2005**, *102*, 15752−15756.
(13) Yelin, D.; Oron, D.; Thiberge, S.; Moses, E.; Silberberg, Y. Multiphoton Plasmon-Resonance Microscopy. *Opt. Express* **2003**, *11*, 1385−1391.
(14) Mohamed, M. B.; Volkov, V.; Link, S.; El-Sayed, M. A. The "Lightning" Gold Nanorods: Fluorescence Enhancement of over a Million Compared to the Gold Metal. *Chem. Phys. Lett.* **2000**, *317*, 517−523.
(15) Kovtyukhova, N. I.; Mallouk, T. E. Nanowires as Building Blocks for Self-Assembling Logic and Memory Circuits. *Chem.—Eur. J.* **2002**, *8*, 4355−4363.
(16) Huschka, R.; Zuloaga, J.; Knight, M. W.; Brown, L. V.; Nordlander, P.; Halas, N. J. Light-Induced Release of DNA from Gold Nanoparticles: Nanoshells and Nanorods. *J. Am. Chem. Soc.* **2011**, *133*, 12247−12255.
(17) Khalavka, Y.; Becker, J.; Sonnichsen, C. Synthesis of Rod-Shaped Gold Nanorattles with Improved Plasmon Sensitivity and Catalytic Activity. *J. Am. Chem. Soc.* **2009**, *131*, 1871−1875.
(18) Love, J. C.; Estroff, L. A.; Kriebel, J. K.; Nuzzo, R. G.; Whitesides, G. M. Self-Assembled Monolayers of Thiolates on Metals as a Form of Nanotechnology. *Chem. Rev.* **2005**, *105*, 1103−1169.
(19) Vericat, C.; Vela, M. E.; Benitez, G.; Carro, P.; Salvarezza, R. C. Self-Assembled Monolayers of Thiols and Dithiols on Gold: New Challenges for a Well-Known System. *Chem. Soc. Rev.* **2010**, *39*, 1805−1834.
(20) Brust, M.; Walker, M.; Bethell, D.; Schiffrin, D. J.; Whyman, R. Synthesis of Thiol-Derivatized Gold Nanoparticles in a 2-Phase Liquid-Liquid System. *J. Chem. Soc., Chem. Commun.* **1994**, 801−802.
(21) Bain, C. D.; Troughton, E. B.; Tao, Y. T.; Evall, J.; Whitesides, G. M.; Nuzzo, R. G. Formation of Monolayer Films by the Spontaneous Assembly of Organic Thiols from Solution Onto Gold. *J. Am. Chem. Soc.* **1989**, *111*, 321−335.
(22) Mirkhalaf, F.; Paprotny, J.; Schiffrin, D. J. Synthesis of Metal Nanoparticles Stabilized by Metal-Carbon Bonds. *J. Am. Chem. Soc.* **2006**, *128*, 7400−7401.
(23) Atmane, Y. A.; et al. Functionalization of Aluminum Nanoparticles Using a Combination of Aryl Diazonium Salt Chemistry and Iniferter Method. *J. Phys. Chem. C* **2013**, *117*, 26000−26006.
(24) Griffete, N.; Herbst, F.; Pinson, J.; Ammar, S.; Mangeney, C. Preparation of Water-Soluble Magnetic Nanocrystals Using Aryl Diazonium Salt Chemistry. *J. Am. Chem. Soc.* **2011**, *133*, 1646−1649.
(25) Laurentius, L.; Stoyanov, S. R.; Gusarov, S.; Kovalenko, A.; Du, R. B.; Lopinski, G. P.; McDermott, M. T. Diazonium-Derived Aryl Films on Gold Nanoparticles: Evidence for a Carbon-Gold Covalent Bond. *ACS Nano* **2011**, *5*, 4219−4227.
(26) Adenier, A.; Barre, N.; Cabet-Deliry, E.; Chausse, A.; Griveau, S.; Mercier, F.; Pinson, J.; Vautrin-Ul, C. Study of the Spontaneous Formation of Organic Layers on Carbon and Metal Surfaces from Diazonium Salts. *Surf. Sci.* **2006**, *600*, 4801−4812.
(27) Combellas, C.; Kanoufi, F.; Pinson, J.; Podvorica, F. I. Time-of-Flight Secondary Ion Mass Spectroscopy Characterization of the Covalent Bonding Between a Carbon Surface and Aryl Groups. *Langmuir* **2005**, *21*, 280−286.
(28) Mesnage, A.; Lefevre, X.; Jegou, P.; Deniau, G.; Palacin, S. Spontaneous Grafting of Diazonium Salts: Chemical Mechanism on Metallic Surfaces. *Langmuir* **2012**, *28*, 11776−11787.
(29) Nikoobakht, B.; El-Sayed, M. A. Preparation and Growth Mechanism of Gold Nanorods (Nrs) Using Seed-Mediated Growth Method. *Chem. Mater.* **2003**, *15*, 1957−1962.
(30) Almora-Barrios, N.; Novell-Leruth, G.; Whiting, P.; Liz-Marzan, L. M.; Lopez, N. Theoretical Description of the Role of Halides, Silver, and Surfactants on the Structure of Gold Nanorods. *Nano Lett.* **2014**, *14*, 871−875.
(31) Hubert, F.; Testard, F.; Spalla, O. Cetyltrimethylammonium Bromide Silver Bromide Complex as the Capping Agent of Gold Nanorods. *Langmuir* **2008**, *24*, 9219−9222.
(32) Jackson, S. R.; McBride, J. R.; Rosenthal, S. J.; Wright, D. W. Where's Silver? Imaging Trace Silver Coverage on the Surface of the Gold Nanorods. *J. Am. Chem. Soc.* **2014**, *136*, 5261−5263.
(33) Niidome, Y.; Nakamura, Y.; Honda, K.; Akiyama, Y.; Nishioka, K.; Kawasaki, H.; Nakashima, N. Characterization of Silver Ions Adsorbed on Gold Nanorods: Surface Analysis by Using Surface-Assisted Laser Desorption/Ionization Time-of-Flight Mass Spectrometry. *Chem. Commun.* **2009**, 1754−1756.
(34) Orendorff, C. J.; Murphy, C. J. Quantitation of Metal Content in the Silver-Assisted Growth of Gold Nanorods. *J. Phys. Chem. B* **2006**, *110*, 3990−3994.
(35) Liu, M. Z.; Guyot-Sionnest, P. Mechanism of Silver(I)-Assisted Growth of Gold Nanorods and Bipyramids. *J. Phys. Chem. B* **2005**, *109*, 22192−22200.
(36) Laforgue, A.; Addou, T.; Belanger, D. Characterization of the Deposition of Organic Molecules at the Surface of Gold by the Electrochemical Reduction of Aryldiazonium Cations. *Langmuir* **2005**, *21*, 6855−6865.
(37) Doppelt, P.; Hallais, G.; Pinson, J.; Podvorica, F.; Verneyre, S. Surface Modification of Conducting Substrates. Existence of Azo Bonds in the Structure of Organic Layers Obtained from Diazonium Salts. *Chem. Mater.* **2007**, *19*, 4570−4575.
(38) Liu, Y. C.; McCreery, R. L. Raman Spectroscopic Determination of the Structure and Orientation of Organic Monolayers Chemisorbed on Carbon Electrode Surfaces. *Anal. Chem.* **1997**, *69*, 2091−2097.
(39) Hurley, B. L.; McCreery, R. L. Covalent Bonding of Organic Molecules to Cu and Al Alloy 2024 T3 Surfaces Via Diazonium Ion Reduction. *J. Electrochem. Soc.* **2004**, *151*, B252−B259.
(40) Boca, S. C.; Astilean, S. Detoxification of Gold Nanorods by Conjugation with Thiolated Poly(Ethylene Glycol) and Their Assessment as Sers-Active Carriers of Raman Tags. *Nanotechnology* **2010**, *21*, 235601.
(41) R. A, Frisch, M. J.; Trucks, G. W.; Schlegel, H. B.; Scuseria, G. E.; Robb, M. A.; Cheeseman, J. R.; Scalmani, G.; Barone, V.; Mennucci, B.; Petersson, G. A.; Nakatsuji, H.; Caricato, M.; Li, X.; Hratchian, H. P.; Izmaylov, A. F.; Bloino, J.; Zheng, G.; Sonnenberg, J. L.; Hada, M.; Ehara, M.; Toyota, K.; Fukuda, R.; Hasegawa, J.; Ishida, M.; Nakajima, T.; Honda, Y.; Kitao, O.; Nakai, H.; Vreven, T.;

Montgomery, Jr., J. A.; Peralta, J. E.; Ogliaro, F.; Bearpark, M.; Heyd, J. J.; Brothers, E.; Kudin, K. N.; Staroverov, V. N.; Kobayashi, R.; Normand, J.; Raghavachari, K.; Rendell, A.; Burant, J. C.; Iyengar, S. S.; Tomasi, J.; Cossi, M.; Rega, N.; Millam, J. M.; Klene, M.; Knox, J. E.; Cross, J. B.; Bakken, V.; Adamo, C.; Jaramillo, J.; Gomperts, R.; Stratmann, R. E.; Yazyev, O.; Austin, A. J.; Cammi, R.; Pomelli, C.; Ochterski, J. W.; Martin, R. L.; Morokuma, K.; Zakrzewski, V. G.; Voth, G. A.; Salvador, P.; Dannenberg, J. J.; Dapprich, S.; Daniels, A. D.; Farkas, Ö.; Foresman, J. B.; Ortiz, J. V.; Cioslowski, J.; Fox, D. J. *Gaussian 09*; Gaussian, Inc.: Wallingford, CT, 2009.

(42) Becke, A. D. Density-Functional Thermochemistry 0.3. The Role of Exact Exchange. *J. Chem. Phys.* **1993**, *98*, 5648−5652.

(43) Lee, C. T.; Yang, W. T.; Parr, R. G. Development of the Colle-Salvetti Correlation-Energy Formula Into a Functional of the Electron-Density. *Phys. Rev. B* **1988**, *37*, 785−789.

(44) Clark, T.; Chandrasekhar, J.; Spitznagel, G. W.; Schleyer, P. V. Efficient Diffuse Function-Augmented Basis Sets for Anion Calculations. III. The 3-21+G Basis Set for First-Row Elements, Li-F. *J. Comput. Chem.* **1983**, *4*, 294−301.

(45) Francl, M. M.; Pietro, W. J.; Hehre, W. J.; Binkley, J. S.; Gordon, M. S.; Defrees, D. J.; Pople, J. A. Self-Consistent Molecular-Orbital Methods 0.23. A Polarization-Type Basis Set for 2nd-Row Elements. *J. Chem. Phys.* **1982**, *77*, 3654−3665.

(46) Hay, P. J.; Wadt, W. R. Abinitio Effective Core Potentials for Molecular Calculations - Potentials for the Transition-Metal Atoms Sc to Hg. *J. Chem. Phys.* **1985**, *82*, 270−283.

(47) Fairchild, S. Z.; Bradshaw, C. F.; Su, W. S.; Guharay, S. K. Predicting Raman Spectra Using Density Functional Theory. *Appl. Spectrosc.* **2009**, *63*, 733−741.